Fundamental and harmonic microbunching in a high-gain self-amplified spontaneous-emission free-electron laser

A. Tremaine,[1,2] X. J. Wang,[1] M. Babzien,[1] I. Ben-Zvi,[1] M. Cornacchia,[3] A. Murokh,[2] H.-D. Nuhn,[3] R. Malone,[1] C. Pellegrini,[2] S. Reiche,[2] J. Rosenzweig,[2] J. Skaritka,[1] and V. Yakimenko[1]

[1]*NSLS, Brookhaven National Lab, Upton, New York 11973*

[2]*Department of Physics and Astronomy, UCLA, Los Angeles, California 90095*

[3]*SSRL, SLAC, Stanford, California 94309*

(Received 14 March 2002; published 30 September 2002)

Electron beam microbunching in both the fundamental and second harmonic in a high-gain self-amplified spontaneous emission free-electron laser (SASE FEL) was experimentally characterized using coherent transition radiation. The microbunching factors for both modes (b_1 and b_2) approach unity, an indication of FEL saturation. These measurements are compared to the predictions of FEL simulations. The simultaneous capture of the microbunching and SASE radiation for individual micropulses correlate the longitudinal electron beam structure with the FEL gain.

DOI: 10.1103/PhysRevE.66.036503 PACS number(s): 41.60.Cr, 41.60.Ap, 41.85.Ja

Significant progress has been recently achieved in the worldwide effort of self-amplified spontaneous-emission free-electron laser (SASE FEL) research and development; saturation [1–3] and nonlinear harmonic radiation [4,5] have been observed from the near infrared to UV wavelengths. A signature of the high-gain FEL is the microbunching of the longitudinal electron beam distribution with a periodicity of the FEL's fundamental wavelength. By measuring the degree to which the electron beam is microbunched, important microscopic properties of the SASE radiation system can be determined. A tightly microbunched system, characteristic of FEL saturation, will contain a microbunching structure rich in harmonics, and this harmonic microbunching will drive the nonlinear harmonic radiation (NHR). NHR, for example, can be utilized in proposed x-ray FEL's to attain coherent, harder x rays compared to those of the fundamental radiation.

Observations were made on fundamental SASE FEL microbunching using coherent transition radiation (CTR) [6–8] and also on an FEL oscillator using other methods [9]. A direct correlation between the SASE FEL output and electron beam longitudinal microbunching (determined by CTR) is presented in this paper; both the fundamental and second harmonic microbuching factors are captured from the same micropulse as the SASE radiation over the full range of FEL gain. Details of the harmonic microbunching measurements in a SASE FEL, which drive NHR, are presented. Bunching factors for both the fundamental and second harmonic are experimentally characterized, and compared with SASE FEL theory and computer simulation. The results presented in this paper verify that the fundamental microbunching drives the SASE FEL gain, harmonic microbunching, and nonlinear harmonic generation.

An intense relativistic electron beam propagating through a periodic magnetic undulator may undergo a radiation-producing interaction termed the SASE FEL instability [10]. This instability proceeds by generating light at the FEL's resonant wavelength, and allows the beam to microbunch at the same wavelength. This process has a positive feedback, as microbunching stimulates more *coherent* radiation production. As this process evolves and the electron beam continues to microbunch further, the coherence of the radiated field increases, and the SASE power grows exponentially along the undulator, $P \propto P_0 \exp(z/L_g)$. Here, P_0 is usually taken as the coherent fraction of the spontaneous radiation in the first field gain length, z is the distance along the undulator, and L_g is the power gain length. When the exponential growth in radiated power ends (levels off), the FEL is in a state termed saturation [11]. At saturation, the beam is most densely microbunched, and further coherent power generation is mitigated. As saturation is approached, the modulation of the beam current becomes deep and nonsinusoidal, with significant higher harmonic content. Thus the onset of FEL saturation is accompanied by the presence of significant harmonics [11–13], both in the FEL light generated and the longitudinal electron beam distribution.

The wavelengths at which the electron beam is microbunched, λ_{mb}, are given by

$$\lambda_{\mathrm{mb},n} = \lambda_{r,n} = \frac{\lambda_u}{2\gamma^2 n}\left(1 + \frac{K^2}{2}\right), \tag{1}$$

where λ_u is the undulator period, γ is the electron beam energy, K is the undulator parameter, and $n = 1,2,3,...$, and $n = 1$ corresponding to the fundamental mode. The harmonic microbunching will generate radiation at the same wavelength, $\lambda_{r,n}$, and because of the nature of the radiative process in a planar undulator FEL, odd harmonic radiation production is favored [13]. Because the higher harmonic SASE process is driven by the fundamental microbunching, it is termed NHR. The growth of the NHR starts later in the undulator compared to that of the fundamental, as the fundamental must have considerable gain before the harmonic microbunching can develop. Experimental observation of NHR on the visible to infrared SASE amplifier (VISA) FEL has been reported [4].

The theory of CTR and its application to longitudinal microbunching measurements of electron beams has been extensively studied [6–8,14,15]. A more physical picture of the process, known as the virtual photon, or the Weizsacker-

Williams method [16], can also be used to give the same predictions concerning CTR microbunching [15]. Both analysis assume the beam charge distribution at the exit of a SASE FEL is

$$\rho(x,y,z)=\frac{eN\exp\left(-\frac{x^2}{2\sigma_x^2}-\frac{y^2}{2\sigma_y^2}-\frac{z^2}{2\sigma_z^2}\right)}{(2\pi)^{3/2}\sigma_x\sigma_y\sigma_z}\times\left[1+\sum_{n=1}^{\infty}b_n\cos(nk_rz)\right], \tag{2}$$

where N is the number of electrons in the bunch, $\sigma_{x,y,z}$ are the transverse (x,y) and longitudinal (z) beam sizes, respectively, k_r is the fundamental wave number from Eq. (1), n is the harmonic number, and b_n is the microbunching factor for the nth harmonic. The analysis for CTR assumes that the microbunching period in the beam's rest frame is small compared to the transverse beam size, i.e., $k_r\sigma_{x,y}/\gamma\gg 1$, which is indeed the case for this FEL. For a given harmonic the CTR energy emitted when the electron beam strikes a conducting surface may be obtained using both traditional (annihilation) [6,14] and virtual photon models [15],

$$U_n=\frac{N^2e^2b_n^2}{8\sqrt{\pi}\sigma_x\sigma_y\sigma_z}\left(\frac{\gamma}{nk_r}\right)^4\left(\frac{1}{\sigma_x^2}+\frac{1}{\sigma_y^2}\right). \tag{3}$$

Predictions from Eq. (3) will be compared to the experimental results and simulations when determining the microbunching fractors, b_n. Equation (3) shows that CTR from the harmonic microbunching is reduced significantly from that of the fundamental due to its strong dependence on nk_r.

The SASE FEL microbunching experiments reported here were performed using the VISA FEL, located at Brookhaven National Laboratory's accelerator test facility (ATF). The VISA FEL saturated, with optimum electron beam conditions, before the end of a 4-meter-long permanent magnet undulator. The VISA undulator has a period of 1.8 cm, built in strong focusing and an undulator parameter $K=1.26$ [17]. The high brightness beam used to drive the VISA FEL is generated from a 1.6 cell *S*-band photoinjector. A beam energy of 71 MeV is obtained after acceleration through two SLAC-type traveling wave accelerator sections [18]. The beam is then delivered to the VISA undulator through a matching beamline [2].

The microbunching diagnostic station was installed 30 cm downstream of the undulator exit and consists of a thin aluminum foil and a $\frac{1}{2}$ in. laser quality mirror, separated by $\approx$2.2 cm. The light-tight 6 μm foil is used to separate the SASE radiation from the CTR, as shown in the schematic given in Fig. 1. The SASE radiation is reflected downward from the front surface of the foil. Back-emitted CTR from the front surface of the foil is also emitted downward and is negligible since it has at least three orders of magnitude less energy than the SASE. Both forward CTR (from the back surface of the foil) and the back-emitted CTR (from the mirror) are directed into the microbunching detector. The beam and relevant FEL parameters at the foil are given in Table I.

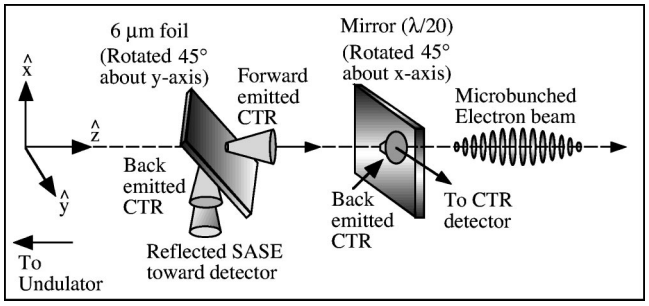

FIG. 1. CTR microbunch monitor. System simultaneously captures CTR (microbunching) and SASE.

Calibrated joulemeters were used for measuring both the SASE and CTR signals. To select a desired microbunching signal, bandpass filters with known spectral responses (centered at 850 and 415 nm with 50 and 10 nm bandwidths, respectively) were positioned before the CTR detector. To minimize the possibility of cross contamination in each measurement, two filters were employed, resulting in an attenuation at least six orders of magnitude outside the bandpass.

Three factors must be taken into consideration when analyzing the measured microbunching factors. First, the electron beam propagates 30 cm after the undulator exit before reaching the foil. At saturation, the electron beam is optimally microbunched and has a large energy spread, causing the electrons to debunch in the drift space. This leads to a reduction of the bunching factors. In addition, the beam expands transversely after exiting the strong-focusing undulator, Eq. (3) indicates that this transverse expansion significantly degrades the CTR energy. The computer code GENESIS [19] was used to study these effects. GENESIS simulates the VISA FEL interaction and electron beam dynamics through the postundulator drift space. Second, the electron beam propagates through the foil before creating part of the measured CTR. Thin-target scattering effects in the foil induce transverse motion in the electrons that can reduce the CTR generated [6]. For the 45° positioned cases, 6 μm foil and the parameters given in Table I, the CTR energy is reduced by about 35% for both the fundamental and second harmonic. And finally, we note the two CTR sources in Fig. 1. The effects of TR interference between two parallel foils are examined in Ref. [20]. When the fields from the two sources combine, those emitted from the mirror will have an additional spatially dependent phase. As this phase varies strongly over the emission at the mirror, due to the use of nonparallel emitters, the interference between the two CTR sources is diminished. Furthermore, the foil used here has significant surface roughness. The CTR emission from the

TABLE I. Electron beam and FEL parameters at microbunching diagnostic, 30 cm after undulator.

Beam Energy γ	139
Fundamental wavelength $\lambda_{r,1}$	845 nm
Spot size σ_x, σ_y	60 μm, 120 μm
Pulse length, σ_z	54 μm
Charge Q	145 pC

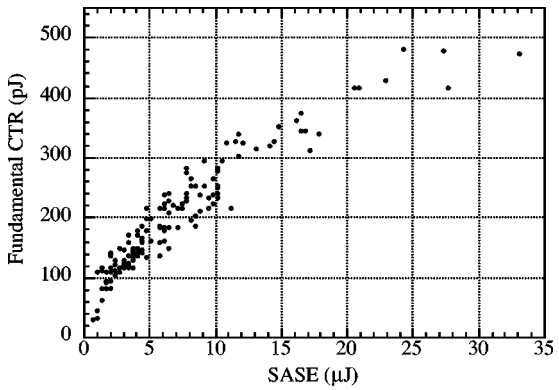

FIG. 2. Measured fundamental CTR vs SASE. Beam is longitudinally microbunched at a period of 845 nm.

foil is more diffuse than that from the mirror, and the overlap of the two CTR signals necessary for interference is again significantly reduced. The lack of CTR interference was confirmed when a charge coupled device camera focused onto the far field onto a similar microbunching monitor observed no interference pattern, but a strong CTR signal; the CTR collected from the foil and mirror add independently.

To understand the relation between the microbunching and radiation in a SASE FEL, we first examine the qualitative nature of the CTR energy U_n as a function of the SASE energy, U_{SASE}. Both the fundamental CTR energy U_1 and U_{SASE} were captured simultaneously for many micropulses, and Fig. 2 shows these measurements. This is a shot-to-shot measurement from low FEL gain to saturation. During exponential gain, we expect both U_1 and U_{SASE} to be proportional to b_1^2 and observe that they are indeed proportional to each other before saturation (lower SASE energies in Fig. 2). This measurement confirms that microbunching is integral to the SASE gain process and that the fundamental microbunching and SASE radiation have the same exponential dependence (growth rate) [10],

$$b_1^2 \propto E_{\mathrm{SASE}} \propto \exp\left(\frac{z}{L_{g,1}}\right), \tag{4}$$

where $L_{g,1}$ is the gain length for the fundamental SASE radiation. A fundamental SASE growth rate, $L_{g,1} \approx 19$ cm, for this FEL has been reported [2,4]. The range of SASE values in Fig. 2 comes not only from SASE statistics, but also fluctuations in the electron beam due to system instabilities. These fluctuations are inconsequential, however, since both the SASE and microbunching (CTR) are measured for every micropulse; a unique microbunching factor can be attributed to each SASE shot.

Simultaneous measurement of the CTR and SASE energies provides another technique in which SASE FEL saturation can be verified independently. At high U_{SASE} and above saturation in Fig. 2, the proportionality described by Eq. (4) is missing. Even though marginally more SASE radiation is produced in the undulator, the lack of increase in the microbunching is further evidence that the FEL is in saturation. To compare these results to a microscopic model of the beam, GENESIS was used to simulate the FEL and post undulator drift, where the particle input used comes from previous simulations of the injector and beam transport to the undulator [2]. Figure 3 plots the microbunching factor b_1 as a function of z, as calculated from GENESIS for the case with near-optimal gain. When the FEL enters saturation before the undulator end, no further microbunching occurs, confirming the measurement in Fig. 2. These simulations predict that b_1 is reduced to $b_1 = 0.52$ at the diagnostic station from its optimum value, $b_1 = 0.60$, immediately preceding the undulator exit. Using the parameters in Table I, data in Fig. 2, and including foil scattering effects [6], Eq. (3) predicts a measured bunching factor $b_1 = 0.50$, which is in close agreement with simulations.

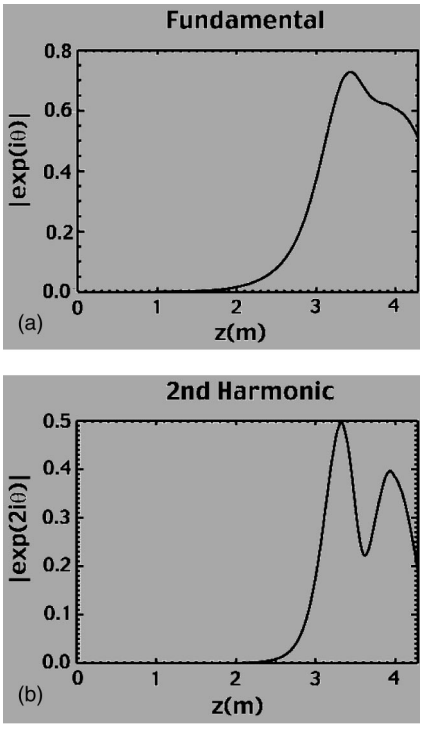

FIG. 3. GENESIS simulations. (a) Fundamental bunching b_1 vs z at peak FEL gain. (b) Second harmonic bunching b_2 vs z at peak FEL gain. Debunching observed during the 30 cm drift after the undulator.

Figure 4 shows measurements of the second harmonic longitudinal microbunching, U_2, vs U_{SASE}. The unfiltered SASE energy is dominated by the fundamental since higher harmonics account only for about 1% of the fundamental [4]. Again at high U_{SASE}, the second harmonic microbunching stops growing, an indication that the beam is not microbunching further. Simulations in Fig. 3 show the second harmonic microbunching, b_2, as a function of z. Once again at saturation, the harmonic microbunching stops growing, confirming the trend shown in Fig. 4.

The microbunching on the second harmonic can be related to that on the fundamental using the theoretical prediction [11] $b_2^2 \propto \exp(z/L_{g,2}) \propto \exp(2z/L_{g,1}) \propto b_1^4$. Here, the radiation gain length for the second nonlinear harmonic, is related to that of the fundamental by $L_{g,2} \cong L_{g,1}/2$. This relationship, verified experimentally at VISA [4], means that U_2 should be quadratic with U_{SASE}. The data show that U_2 is a stronger

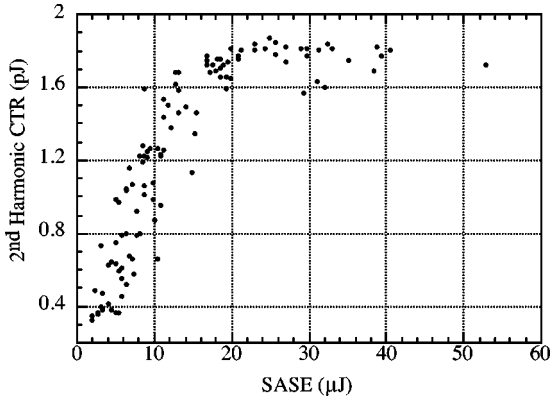

FIG. 4. Measured second harmonic CTR vs SASE. The beam is longitudinally microbunched at a period of 422 nm in addition to 845 nm in Fig. 2.

function of U_{SASE} than is the fundamental microbunching signal, U_1, but establishing a quadratic dependence from the relatively small portion of the data before the saturation of U_2 is difficult.

To generate a prediction for the expected bunching factor, we refer to the GENESIS results displayed in Fig. 3. The bunching factor at the foil is, $b_2=0.2$, reduced from $b_2=0.40$ at the undulator exit. Using the measurements from Fig. 4, the measured peak harmonic bunching factor calculated from Eq. (3) is $b_2=.13$. The discrepancy between predicted and measured microbunching may be due to a variety of factors, such as the uncertainty in the debunching, to which higher harmonics are more sensitive. Also, the assumption of a Gaussian electron beam longitudinal distribution may also have contributed since the real bunch shape displays some non-Gaussian structure [2].

The difficulty in obtaining information about higher harmonic microbunching is further demonstrated by the search for the third harmonic (280 nm) CTR signal, inspired by previous observation of the third nonlinear harmonic SASE signal [4]. Bandpass filters for the third harmonic were situated in front of the CTR detector, but no conclusive signal was measured. Equation (3) predicts a detectable signal (down from the fundamental by a factor of 81), but GENESIS predicts that the effect of the debunching on b_3 reduces the CTR by another factor of 10 on the third harmonic, rendering the signal undetectable.

In conclusion, the dependence of the longitudinal microbunching up to the second harmonic on the observed SASE FEL gain into saturation has been measured using CTR. For single micropulses traversing the undulator, SASE energy and b_1, b_2 were simultaneously measured. The linear proportionality of U_1 on SASE energy up to saturation is clearly established, as is the lack of further microbunching growth after saturation. The linear relationship between the fundamental microbunching and SASE growth is evidence the fundamental microbunching drives the FEL radiation. For the fundamental microbunching measurements the experimental results were in excellent agreement with the predictions of CTR theory and FEL simulations. The second harmonic microbunching appears strongly in this SASE FEL near saturation, as expected. Less impressive agreement was obtained for the second harmonic microbunching case due to uncertainties in debunching, transverse beam expansion, and a possible need to generalize CTR theory. In addition, the two lowest microbunching factors (b_1 and b_2) were characterized; the electrons in the beam are strongly bunched at 845 and 422 nm. These results show the dependence of SASE gain and nonlinear harmonic radiation on the longitudinal structure of the electron beam, the driving mechanism of an FEL.

We would like to express our gratitude to D. Davis for his technical support. This work was partially supported by the U.S. DOE under Grant Nos. DE-AC02-98CH10886 and DE-FG-98ER45693.

[1] S. Milton *et al.*, Science **292**, 2037 (2001).
[2] A. Murokh *et al.* (unpublished).
[3] V. Ayvazyan *et al.* Phys. Rev. Lett. **88**, 104802 (2002).
[4] A. Tremaine *et al.*, Phys. Rev. Lett. **88**, 204801 (2002).
[5] S. G. Biedron *et al.* Nucl. Instrum Methods Phys. Res. A **483**, 94 (2002).
[6] A. Tremaine *et al.*, Phys. Rev. Lett. **81**, 5816 (1998).
[7] A. H. Lumpkin *et al.*, Phys. Rev. Lett. **86**, 79 (2001).
[8] A. H. Lumpkin *et al.*, Phys. Rev. Lett. **88**, 234801 (2002).
[9] K. Ricci and T. Smith, Phys. Rev. ST Accel. Beams **3**, 032801 (2000).
[10] R. Bonifacio, C. Pellegrini, and L. Narducci, Opt. Commun. **50**, 373 (1984).
[11] R. Bonifacio *et al.*, Nucl. Instrum. Methods Phys. Res. A **293**, 627 (1990).
[12] J. B. Murphy, C. Pellegrini, and R. Bonifacio, Opt. Commun. **53**, 187 (1985).
[13] Z. Huang and K. J. Kim, Phys. Rev. E **62**, 7295 (2000).
[14] J. Rosenzweig, G. Travish, and A. Tremaine, Nucl. Instrum. Methods Phys. Res. A **365**, 255 (1995).
[15] A. Tremaine, Ph.D. thesis, University of California, Los Angeles, 1999.
[16] J. D. Jackson, *Classical Electrodynamics*, 2nd ed. (Wiley, New York, 1975).
[17] R. Carr *et al.*, Phys. Rev. ST Accel. Beams **4**, 122402 (2001).
[18] X. J. Wang *et al.*, Phys. Rev. E **54**, R3121 (1996).
[19] S. Reiche, Nucl. Instrum. Methods Phys. Res. A **429**, 243 (1999).
[20] L. Wartski *et al.*, J. Appl. Phys. **46**, 3644 (1975).